Progress of Nonequilibrium Solidification Theory

Qingchun LI†, *Chengsong CUI and Daming XU*
Harbin Institute of Technology, Harbin 150001, China
Xiaoguang YUAN
Jilin University of Technology, Changchun 130025, China

[Manuscript received November 10, 1997, in revised form January 9, 1998]

This paper summarized the theory related to nucleation, interface kinetics, micromorphology evolution and microscopic growth during nonequilibrium alloy solidification. Methods for quantitative analysis of nucleation rate, the criterion of marginal stability, nonequilibrium partition coefficient, as well as the relationship between growth rate with undercooling and dendrite tip radius are presented. Some limitations and future developments of nonequilibrium theory are pointed out.

1. Introduction

Recent years, solidification technique has been developed into a new stage with the development of rapid solidification, improvement of directional solidification and monocrystalline technique, and application for continuous casting technique. The composite materials, gradient materials and functional or structural materials with the microstructure of amorphous, quasicrystal, microcrystal and nanocrystal possess many excellent properties, which meet the everlasting needs for the development of industries. For the conventional solidification theories can not explain and predict the structure of the materials prepared by the modern solidification techniques, nonequilibrium solidification theory has been developed quickly during the past few decades. The quantitative explanation of solidification process has been improved by thermal transmission, mass transfer and the kinetics of moving S/L interface. The absolute stability of planar interface has been perfected by considering some comprehensive criterion for transition of crystal morphology. A quantitative explanation of crystal growth has been developed from the low rate to the high rate. The nonequilibrium theories supply a basis for the analysis of solidification process and design of alloy composition. In this article the current research progress in nucleation, transformation of crystal morphology and growth is reviewed.

2. Nucleation and Selection of Phase

2.1 Nucleation

Conventional solidification theories describe nucleation with two manners, *i.e.* homogeneous nucleation and heterogeneous nucleation. The nucleation in the practical solidification process is that the heterogeneous nucleus can form at low degree of undercooling which restrains the homogeneous nucleation.

The basic theory of heterogeneous nucleation has been outlined by Turnbull and Fisher[1]. The initial nucleation site density n_o within the melt will decrease as nucleation proceeds: the nucleation rate $\dot{n}$ at a given undercooling , ΔT, is given by[1]

$$\dot{n} = K_1 \cdot [n_o - n(t)] \cdot \exp[\frac{-K_2}{T \cdot (\Delta T)^2}] \qquad (1)$$

where K_1 is a coefficient proportional to the collision frequency of the atoms of the melt with the nucleation sites of the heterogeneous particles; K_2 is related to the interfacial energy balance between the nucleus, the liquid, and the foreign substrate on which nucleation occurs.

Although this nucleation theory has been applied to the modeling of equiaxed solidification recently[2,3], it fails to predict the correct grain size[4]. The reason for this failure is summarized in Fig.1. At the small nucleation undercoolings usually encountered in conventional solidification processes (ΔT of the order of 1~10 K), a critical undercooling, ΔT_N, is associated with Eq.(1). Above $T_N (= T_E - \Delta T_N$ or $T_L - \Delta T_N)$, almost no nucleus is formed whereas, as soon as it has been reached, the nucleation density, $n(t)$, quickly increases to the saturation limit given by n_o (see Fig.1). Accordingly, the final grain density is almost independent of the solidification conditions, which have not been found in experiments. For this reason, the modeling of nucleation has recently been reconsidered using the pragmatic approach originally developed by Oldfield[5], but with the additional theoretical background of heterogeneous nucleation behavior shown in Fig.1 occurring at a family of nucleation sites which

† To whom correspondence should be addressed

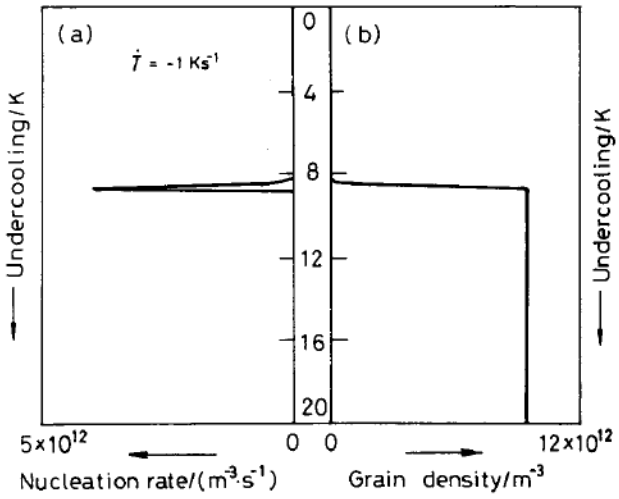

Fig.1 Nucleation rate and grain density as calculated using heterogeneous theory for Al; cooling rate, $\dot{T}$=-1 Ks^{-1}[2] (a) nucleation rate; (b) grain density

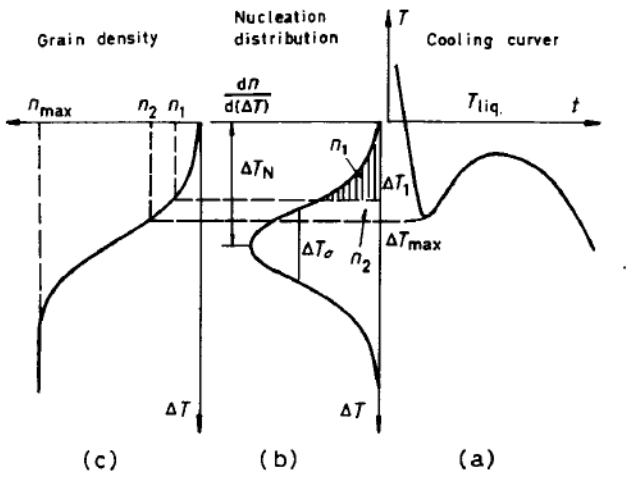

Fig.2 Continuous distribution of nucleation sites used in modeling of equiaxed solidification[6] (a) cooling curve, (b) nucleation distribution, (c) grain density

is characterized by a continuous rather than a discrete distribution, $dn/d(\Delta T)$ (see Fig.2)[6]. At a given undercooling, ΔT_1, [Fig.2(a)], the grain density is given simply by the integral of the nucleation site distribution (*e.g.* Gaussian) from zero undercooling to ΔT_1 [Fig.2(b)]. As Fig.2(c) represents the integral of the nucleation distribution, the grain density n_1, corresponding to ΔT_1, can be obtained directly. By this means, the new grain density is updated at each timestep as a function of the undercooling. When the minimum undercooling of the cooling curve is reached, *i.e.*, when recalescence occurs, this corresponds to the final grain density n_2, associated with the maximum undercooling, ΔT_{max}. The maximum density of nuclei, n_{max}, is given by the integral of the total distribution (from zero undercooling to infinite undercooling). This approach, which has been successfully applied to dendrite[6] and eutectic[7] solidification, could also be applied in order to describe temporal change in an inoculation by assuming an appropriate time dependence of the distribution parameters. Therefore, this model is quite general and can be easily implemented into numerical calculations; without giving convergence problems for the final calculated grain density.

2.2 Selection of phase

Under the nonequilibrium solidification conditions, especially in a rapid solidification process, a large amount of new phases and metastable phases form and can cause the diagram deviating greatly from the equilibrium diagram, so the control and selection for the nonequilibrium phases are an effective way to improve the properties of the alloy. The selection of phase (the order of solid formation) depends on either comparative nucleation rate and comparative growth velocity. Because the competition of nucleation rate between phases plays a crucial role in the selection of phase during nonequilibrium solidification, the incubation period of nucleation decides the type of formed phases. Because the calculation methods of the incubation period of nucleation based on the stable theories do not apply to the rapid solidification process that starts with a large degree of undercooling[8], Shao[9] has obtained the relationship between temperature and nucleation incubation period as

$$\tau = \frac{7.2 \cdot R \cdot f(\theta)}{1-\cos\theta} \cdot \frac{a^4}{d_a^2 \cdot X_{L,eff}} \cdot \frac{T_r}{D_i \cdot S_m \cdot \Delta T_r^2} \quad (2)$$

$$f(\theta) = 0.25(2 - 3\cos\theta + \cos^3\theta)$$

$$T_r = T/T_m, \Delta T_r = 1 - T_r$$

where d_a is the average diameter of atoms in the solid, S_m is the melting entropy per mole, $X_{L,eff}$ is the effective concentration of solute in the melt, D_i is the diffusion coefficient of the solute in the melt, a is the shortest jumping distance of the atoms, θ is contact angle for heterogeneous nucleation, R is the grain radius.

Figure 3 shows the calculated $T-\tau$ curves of Al-Cr alloys by the above mentioned model. The predicted results that the prime phase is $Al_{13}Cr_2$ or $Al_{11}Cr_2$ in Al-Cr alloys with the curves in Fig.3 coincide well with test results[10].

In addition, the factors influencing the selection of phase include the type of the phase and the melting point of the phase as foreign nucleus[11,12], as well as the inheritance form and the thermal history of the melt[13].

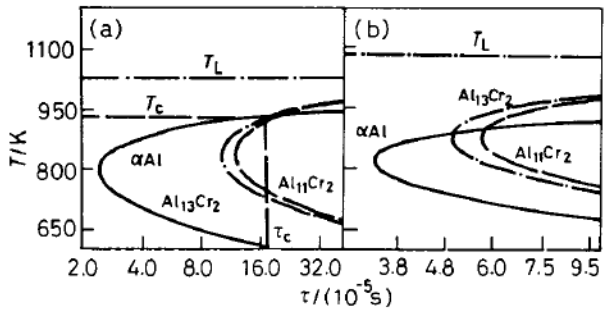

Fig.3 Calculated $T-\tau$ curve[9] (a) Al-1.0%Cr, (b) Al-2.0%Cr (atom fraction)

3. Effect of Nonequilibrium Conditions on the S/L Interface

3.1 Interface movement kinetics

So far it has been assumed that the local equilibrium condition is present at the S/L interface. Strictly speaking, any motion of the interface requires some driving force at the interface which will cause departure from local equilibrium. The driving force required for the motion of the interface can be related to the velocity of the interface through the reaction rate theory of atomic jumps across the interface. Since the driving force is related to the change in the free energy, it can be written in a general form as[14]

$$V = V_0 \cdot [1 - \exp(-\frac{\Delta G_m}{R_g \cdot T_i})] \quad \text{or}$$

$$\Delta G_m = -R_g \cdot T_i \cdot \ln[1 - \frac{V}{V_0}] \tag{3}$$

where ΔG_m is the free energy change per mole required to drive the interface to move, R_g the gas constant, and V_0 a constant which is of the order of the velocity of sound for pure metals. ΔG_m is proportional to the kinetic undercooling, ΔT_k, at the interface, *i.e.*

$$\Delta G_m = \Delta S_m \cdot \Delta T_k \tag{4}$$

where ΔS_m is the entropy change per mole. The kinetic undercooling at the interface is thus obtained as

$$\Delta T_k = -(\frac{R_g \cdot T_i}{\Delta S_m}) \cdot \ln(1 - \frac{V}{V_0}) \tag{5}$$

For $(V/V_0) \ll 1$, and $T_i \cong T_m$, the above relationship can be simplified as

$$V = \mu_k \cdot (\Delta T_k) \tag{6}$$

where $\mu_k [= V_0 \cdot \Delta S_m/(R_g \cdot T_i)]$ is the interface kinetics coefficient. Thus it can be seen that the kinetic undercooling is directly proportional to the velocity of the interface. Because of the high growth velocity at the interface under nonequilibrium conditions, the kinetic undercooling is usually large.

3.2 Thermodynamic constraint

When the local equilibrium is satisfied at the interface, the compositions of the solid and the liquid at the interface are uniquely determined by equating the chemical potentials of solute as well as solvent in the two phases. However, in the absence of local equilibrium, a range of the compositions is possible at the interface. Although equilibrium conditions are no longer valid, the thermodynamic considerations are still important in that the compositions at the interface are restricted to values which give an overall decrease in the free energy[15].

Free energy-composition diagram is shown in Fig.4. The equilibrium compositions, C_{Le} and C_{Se}, are given by the common tangent to the free energy curves for the solid and the liquid. Consider now an arbitrary liquid of composition, C_L. The free energy change when one mole of solid forms from an infinite amount of liquid of composition C_L is obtained by first drawing a tangent at the composition C_L. If the solid that forms has a composition C_S, then the free energy change is given by the distance from the tangent line to the free energy curve for the solid, as shown in Fig.4. For liquid compositions that are greater than C_{Le}, there is no composition of the solid for which a reduction in free energy would occur. For liquid composition C_L, which is less than C_{Le}, only a range of solid compositions is possible for which there is a reduction in the free energy, as shown in Fig.4.

The limiting composition is obtained when the free energy change is zero, *i.e.* where the tangent line first intersects the free energy curve for the solid. The selection of a solid composition smaller than this limiting composition will occur only if some driving force ΔG_m is required for the attachment kinetics. The value of ΔG_m is known for a given velocity through the interface kinetic law that is operative at the interface, *e.g.* Eq.(3) for a linear kinetic law. The magnitude of free energy change for the formation of one mole of solid of composition C_S from a liquid of composition C_L, is given by

$$\Delta G_m = (1 - C_s) \cdot [\mu_{SA}(C_L) - \mu_{LA}(C_L)] + C_S \cdot [\mu_{SB}(C_L) - \mu_{LB}(C_L)] \tag{7}$$

Substituting the values of from Eq.(3) into (7) gives the general equation that relates the composition in the liquid and in the solid at the interface. Based on the free energy ΔG_m, the interface temperature T_i can be obtained as[16]

$$T_i = T_m + m_v \cdot C_L - (\frac{2\Gamma}{R}) - (\frac{V}{\mu_k})$$

$$m_v = m \cdot [1 + \frac{k_0 - k_v + k_v \cdot \ln(k_v/k_0)}{1 - k_0}] \tag{8}$$

where the capillary undercooling term is also included, Γ is Gibbs- Thomson coefficient, m_v is an effective liquidus slope, k_0 and k_v are defined separately as the

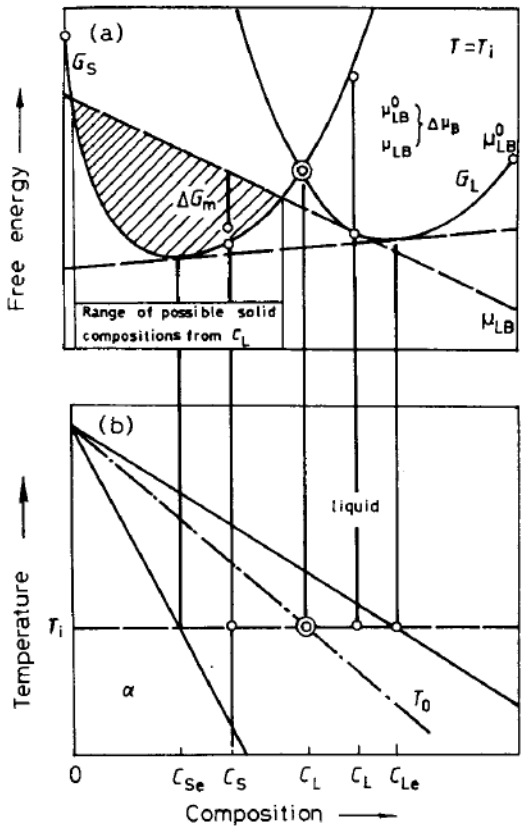

Fig.4 Molar free energy *vs* composition diagram[15]

equilibrium and nonequilibrium ratio of compositions of the solid and the liquid at the S/L interface. For an equilibrium diagram with constant m and k_0, m_v is a function V through k_v. This correction ensures that when k_v approaches one, the liquidus slope approaches the slope of the T_0 line which is defined by equal Gibbs free energy in the solid and liquid.

3.3 Solute partition coefficient

The compositions in the liquid and in the solid at the interface can not be determined by equilibrium diagram under nonequilibrium conditions. Solute partition coefficient, k_v, is a function of the velocity of S/L interface, and effected by the composition and thermal gradient. Baker *et al.*[17] discovered that the maximum solid solubility of Cd in the Zn-Cd alloy prepared by splat quenching of molten alloy is much higher than that by equilibrium solidification technology, which is caused by the high velocity of S/L interface. For this reason, two-level model of solute partition is established, and equation of solute partition coefficient and velocity of S/L interface is obtained as

$$k_v = \frac{(V\cdot a_o/D_i)+\ln k_0}{(V\cdot a_o/D_i)+(1/k_0)\cdot(\ln k_0)}\cdot\frac{1}{\exp(-V\cdot a_o/D_i)} \tag{9}$$

where a_o is the shortest distance between atoms in the melt.

On the basis of chemical rate theory and the detailed balance principle, Aziz[18] has established the nonequilibrium model for solute redistribution during rapid solidification. This model describes quantitatively the relationship between solute partition coefficient and moving velocity of S/L interface at continuous growth. Solute partition coefficient can be obtained as

$$k_v = \frac{V\cdot a_o/D_i + k_e}{1+V\cdot a_o/D_i-(1-k_e)\cdot C^i_L}$$

$$k_e = k_o\cdot(1-C^e_L)/(1-C^e_S) \tag{10}$$

where C^i_L is the solute concentration in the liquid at the interface. C^e_L and C^e_S are the solute concentrations in liquid and in solid separately corresponding to the practical temperature in an equilibrium solidification. Compared with two-level model[17], the calculated result is much close to the test value. Equation (10) can be simplified for dilute solution as following[18]

$$k_v = \frac{k_0+P_c}{1.+P_c} \tag{11}$$

where $P_c(=a_o\cdot V/D_i)$ is the interface Peclet number for solute redistribution. When $V \ll D_i/a_o$, it leads to $P_c \to 0$ and $k_v \to k_0$. Because P_c increases with V, the solute is captured by the growth interface. When $V \gg D_i/a_o$, this leads $P_c \to \infty$ and $k_v \to 1$, it means the solute is captured completely. Therefore, this model can explain the phenomenon of segregation reduction at high growth velocity.

As Aziz made further studying on the effect of nonequilibrium dynamic on the solute partition coefficient, a model of solute redistribution at S/L interface with continuous growth during rapid solidification was obtained as[19]

$$k_v = \frac{(V\cdot a_o/D_i)+k_e(X_L,X_S,T)}{(V\cdot a_o/D_i)+1-(1-k_e)\cdot X_L} \tag{12}$$

where $k_e(X_L,X_S,T)$ is the force of solute redistribution, X_S and X_L are the mole fraction of solute in the solid and liquid respectively.

Even if Aziz model has been widely accepted and quoted by some monographs and papers, the fact that the detailed balance does not hold if a system is far from equilibrium makes the model need to be revised. Chen *et al.*[20] extended the Aziz model using Haken's result[21] and discussed physical variables used in the Aziz model. The revised solute partition coefficient is obtained as

$$k_v = \frac{\beta_f + k_r/k_f}{\beta_f+1} \tag{13}$$

where β_f, k_r and k_f are the dynamic variables. This model predicts the interface velocity at which the solute trapping occurs is greater than that in the Aziz model.

Guo *et al.*[22] have analyzed theoretically the relationship among the solute partition coefficient at a

S/L interface, the temperature gradient and the external force field. The equation of solute partition coefficient that includes many influence factors can be deviated from the value of the equilibrium partition coefficient as

$$k_v = \frac{\beta + k_0 + \alpha_L \cdot G_L + r_L \cdot F_L}{1 + \beta - \alpha_S \cdot G_S - r_S \cdot F_S} \quad (14)$$

where β is the dimensionless velocity, G_L and G_S are the temperature gradient in the liquid and in the solid respectively, α_L and α_S are the temperature gradient coefficient in the liquid and in the solid; F_L and F_S are the external force field in the liquid and in the solid respectively, r_L and r_S are the external force field coefficient in the liquid and in the solid respectively.

Moreover, Wang *et al.*[23] studied the solute redistribution in microgravity field and obtained a solute redistribution model that includes the effect of chemical reaction process at isothermal and equal pressure, Soret effect and growth velocity of interface on the model.

4. Stability and Morphology Transition of the L/S Interface in Nonequilibrium Solidification Conditions

4.1 Dynamic theories of interface stability

The ratio G_L/V which was deduced by theory of constitutional undercooling, can be as a criterion for the stability of L/S interface in equilibrium solidification conditions. The phenomenon that L/S interface planar growth at small value of G_L/V (*i.e.* at high growth velocity) can not be explained with theory of constitutional undercooling during rapid solidification process. Based on an analysis for the solidification dynamic, Mullins *et al.*[24] established a theory of interface stability that is applied more widely than constitutional undercooling, called as dynamic theory of interface stability. The dynamic criterion for the stability of L/S interface can be obtained as

$$S(\omega) = -T_m \cdot \Gamma \cdot \omega^2 - (\bar{K}_L \cdot G_L + \bar{K}_S \cdot G_S) + m \cdot G_C \cdot \frac{\omega_c - V/D_i}{w_c - (V/D_i) \cdot (1 - k_0)}$$

$$\omega_c = V/(2D_i) + \{[V/(2D_i)]^2 + \omega^2\}^{1/2}$$

$$\bar{K}_L = K_L/(K_L + K_S),\ \bar{K}_S = K_S/(K_L + K_S) \quad (15)$$

where G_C is the concentration gradient in the liquid at the planar interface of L/S, ω is wave number, K_L and K_S are the thermal conductivity of liquid and solid respectively.

When $S(\omega)$ is less than zero, the interface of L/S keeps stable; if not, it will be not planar.

Equation (15) shows that $S(\omega)$ depends on the interface velocity under the condition of a constant composition and disturbance

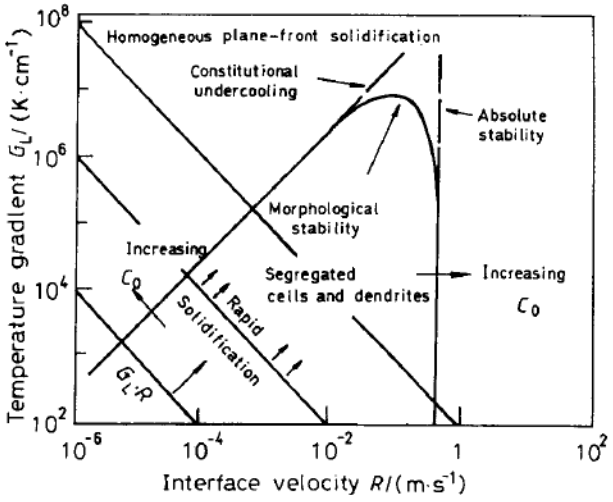

Fig.5 Schematic of absolute stability in change from planar to unstable growth[24]

frequency. If the interface velocity is small, *i.e.* $V/D_i \ll \omega$, and the function of interface energy can be omitted, Eq.(15) can be simplified for the interface stability based on the constitutional undercooling theory. If the interface velocity is large, *i.e.* $V/D_i \gg \omega$, the absolute velocity V_a can be obtained:

$$V_a = \frac{m \cdot C_o(1 - k_0) \cdot C_L}{k_0^2 \cdot \Gamma} \quad (16)$$

The absolute velocity does not depend on the temperature gradient, and increases with the raising of solute composition C_o. Figure 5 shows the relationships between growth velocity, temperature gradient and crystal morphologies for Al-0.1Cu alloy that is calculated with Eq.(15)[25].

Langer *et al.*[26] have also analyzed systematically the stability of interface and established a theory model. Lipton *et al.*[27] have analyzed the effect of undercooling on the interface stability and improved Mullins's model. They divide undercooling into three parts: thermal undercooling, surfacial energy curvature undercooling and constitutional undercooling. The undercooling effects on the interface stability through diffusion coefficient D_i. This means that the diffusion coefficient D_i decreases with the undercooling increasing to raise the stability and reduce V_a.

Trivedi *et al.*[28] gave the interface stability criterion for high Peclet number. When $\dot{\delta}/\delta$ is less than zero, the L/S interface keeps stable; if not, it will be buckling. The equation of the interface stability criterion for pure metal can be expressed:

$$\frac{\dot{\delta}}{\delta} = \frac{K_S \cdot \omega_S + K_L \cdot \omega_L}{\Delta H}[-\Gamma\omega^2 - \frac{K_S \cdot \omega_S \cdot G_S + K_L \cdot \omega_L \cdot G_L}{K_S \cdot \omega_S + K_L \cdot \omega_L} -$$

$$\frac{V \cdot (K_S \cdot G_S/a_S + K_L \cdot G_L/a_L)}{K_S \cdot \omega_S + K_L \cdot \omega_L}] \quad (17)$$

where

$$\omega_c = (V/2D_i) + [(V/2D_i)^2 + \omega^2]^{1/2}$$

$$\omega_L = (V/2a_L) + [(V/2a_L)^2 + \omega^2]^{1/2}$$

$$\omega_S = (V/2a_S) + [(V/2a_S)^2 + \omega^2]^{1/2}$$

δ is amplitude, $\dot{\delta}$ is rate of amplitude change.

According to Eq.(17) the ultimate velocities of interface instability can be obtained:

$$V_c = \frac{G_L \cdot D_i}{\Delta T_o}, \quad V_a = \frac{D_i \cdot \Delta T_i}{\Gamma \cdot k_v} \quad (18)$$

where ΔT_o is the freezing range for the alloy with composition C_o. Therefore, the condition of instability for planar interface is

$$V_c < V < V_a \quad (19)$$

In addition, Wang *et al.*[29] derived the interface stability criterion for binary alloys under the condition of microgravity. They reached the conclusion that the microgravity can increase the stability of interface by suppressing convection and thickening the diffusion boundary layer.

4.2 Evolution of solidification structure morphology

In the rapidly solidified alloys, solidification structure morphologies are mainly dendritic or cellular except featureless structure. The important parameter to describe the crystal morphology is dendrite tip radius R.

Kurz *et al.*[30] gave a descriptive equation for the dendrite tip radius based on Mullins and Sekerka theory[24],

$$R = 2\pi \cdot [\frac{\Gamma}{m \cdot G_c \cdot \xi_c - G_L}]^{1/2} \quad (20)$$

where

$$\xi_c = 1 - \frac{2k_o}{[1 - (2\pi/P_c)^2]^{1/2} - 1 + 2k_o}$$

where P_c is solute Peclet number of dendrite tip.

If the effect of temperature gradient on the diffusion field is neglected, and equilibrium liquidus slope m is replaced by effective liquidus slope m_v, the following equation can be obtained:

$$V \cdot R^2 = \frac{4\pi^2 \cdot D_i \cdot \Gamma \cdot [1 - (1 - k_o) \cdot Iv(P_c)]}{C_o \cdot m_v \cdot (k_v - 1) \cdot \xi_c} \quad (21)$$

where $Iv(P_c)$ is Ivantsov function of P_c.

When Peclet number P_c is small, $\xi_c \to 1$ and $Iv(P_c) \to 0$, Eq.(21) changes into

$$V \cdot R^2 = \frac{4\pi^2 \cdot D_i \cdot k_v}{m_v \cdot C_o \cdot (k_v - 1)} = \text{constant} \quad (22)$$

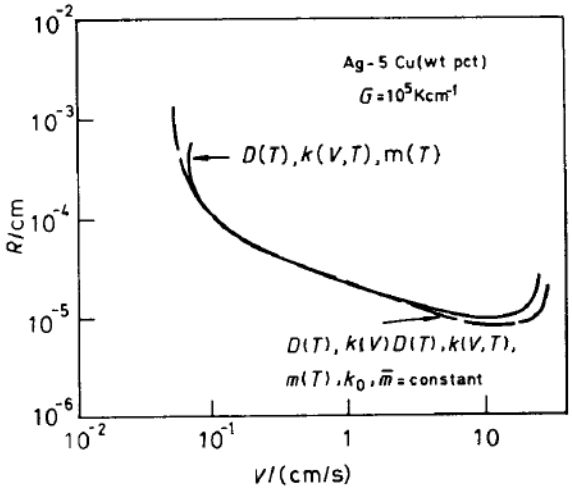

Fig.6 Effect of the phase diagram $k(T), m(T)$ on the $R - V$ relationship for a Ag-5 wt pct Cu alloy at G=10^5 K/cm[30]

For the high Peclet number P_c and ξ_c as a unit, Eq.(21) can be simplified as

$$V \cdot R^2 = \frac{4\pi \cdot D_i \cdot m_v \cdot C_o \cdot (k_v - 1)}{k_v} \quad (23)$$

This is KGT model to describe the crystal morphology, which can be applied to both equilibrium and nonequilibrium solidification. Figure 6 shows the relationship of $R - V$ calculated with KGT model[30].

The calculation results with KGT model coincide with experimental results for dilute solution alloys, but deviate for concentrated solution alloys[28]. Lu *et al.*[31] believed that the reason is neglecting of the change of solute distribution coefficient k_v with composition C_o. So they suggested an improved equation for the liquid composition at dendrite tip. The prediction results for Al-Fe alloy with improved KGT model coincide with the experimental results.

Trivedi *et al.*[28,32] as well as revised KGT model, which refer the method of revising the interface stability, to replace k_v with improved solute distribution coefficient k^* obtained the relationship of $R - V$ for concentrated solute alloys as

$$V \cdot R^2 = \frac{\Gamma \cdot D_i}{\sigma^*} \cdot \Delta T_S \cdot \xi_c^* \quad (24)$$

where σ^* is stability constant, $\Delta T_S = m_v \cdot (C_S - C_L)$, $\xi_c^* = (\omega^* - V/D_i) \cdot [\omega^* - (1 - k^*) \cdot V/D_i]$.

Moreover, Fu[33] and Zhou[34] studied the interface morphology evolution in sub-rapid directional solidification, in which the transitions of dendrite-microcell and microcell-plane have been studied and the evolving laws have been revealed.

Figure 7 shows a schematic variation in the interface temperature with velocity[35].

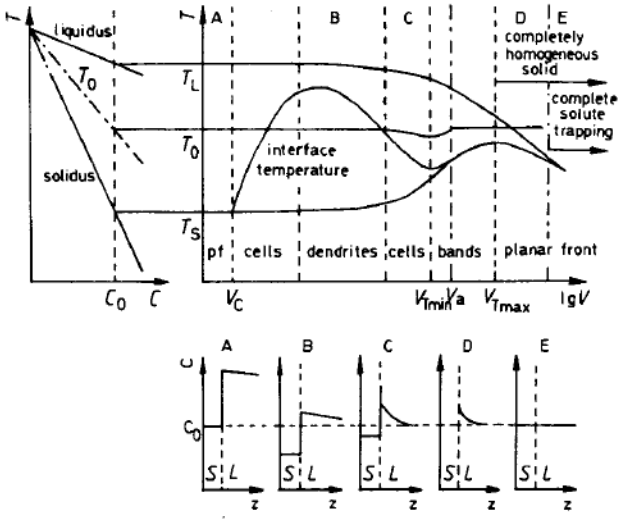

Fig.7 Representation of interface temperature and velocity *vs* micromorphology evolution[35]

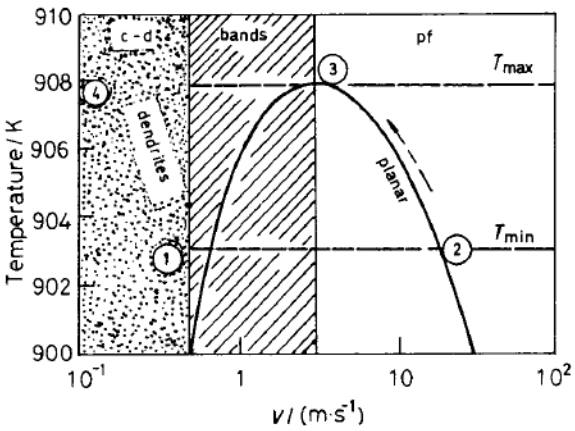

Fig.8 Variation in interface temperature with velocity in high velocity regime[35]

4.3 Formation of banded microstructures

Under rapid solidification conditions, in the regime between the cellular-dendrite and planar front solidification where the absolute stability is predicted by the linear stability analysis[24], the formation of a banded structure which consists of alternate planar front and cellular-dendrite solidification is often observed. These bands are approximately perpendicular to the growth direction. This phenomenon appeared in Al-Fe alloys and other alloys by laser and electron beam treatment, including dendrite and eutectic alloys[36,37].

The formation of a banded structure at high velocities is a consequence of nonequilibrium phenomena which occur at the interface. In order to describe the band formation mechanism, the high velocity regime of Fig.7 is magnified in Fig.8 for clarity. At the cellular to planar front transition V_a, the interface undercooling decreases as the velocity is increased. This inverse relationship between the velocity and the driving force (undercooling) gives rise to instability in which the average velocity of the interface moving equals to the moving velocity of the isotherms in added temperature field. This oscillatory cycle, when the latent heat effect is neglected, is shown in Fig.8.

When the average velocity of the interface, which is equal to the rate of isotherm advance, is between points 1 and 3 in Fig.8, there is no stable steady state solution so that the interface velocity goes through the cycle represented by points 1, 2, 3, and 4. A cellular-dendrite microstructure forms along the curve from point 4 to 1, then the interface accelerates rapidly to point 2, after which it decelerates from point 2 to 3 with a planar front. Finally, when it reaches point 3, it decelerates to point 4 to complete the cycle. Steady state planar front growth is obtained only at velocities beyond the maximum in interface temperature.

This interesting phenomenon has been analyzed by several groups[35,37,38]. Merchant *et al.*[39] have modeled the effects of nonequilibrium solidification on the stability of the plane front. Karma *et al.*[40] have solved the unsteady phenomenon by coupling heat and mass transport to the interface kinetics. Their result confirms the general trend described above but shows a more complicated oscillatory behavior.

5. Growth of Microstructures in Nonequilibrium Conditions

The growth of microstructures can be divided into two types according to the composition of the alloys, eutectic growth and dendrite growth.

In the nonequilibrium conditions, the driving force of eutectic growth — undercooling $\Delta T_{E,e}$ includes eutectic composition undercooling $\Delta T_{E,c}$ and thermal undercooling ΔT_t[41]. Dustin and Kurz[3] established a model for the binary eutectic alloy, and obtained the equation of $\Delta T_{E,e}$:

$$\Delta T_{E,e} = 2(K_c \cdot K_r \cdot V_s)^{1/2} + g \cdot (R/R_o) \cdot R_o \cdot V_s \quad (25)$$

where K_r, K_c and g are constants, V_s is the growth rate of isotherm, R_o is the final grain size. Under equilibrium solidification conditions the model changes into Jackson and Hunt's model for the small thermal undercooling ΔT_t.

The case of ternary eutectic alloys involves yet more complications. For example, when adding Si to an Fe-C alloy so as to remain in the eutectic valley, silicon is depleted within the liquid region ($k > 1$). In the stationary situation of constrained growth, the diffusion layer associated with silicon diffusion modifies the growth equation of the binary eutectics, as demonstrated by McCartney *et al.*[42]. They obtained the following equation for $\Delta T_{E,e}$:

$$\Delta T_{E,e} = 2(k_c \cdot K_r \cdot V_s)^{1/2} + m_x \cdot C_x^* \quad (26)$$

where m_x is the slope of the eutectic valley and C_x^* is the interface concentration of the ternary element in the liquid.

To conclude this section on eutectic growth, the special case of nodular cast iron is briefly presented. When Fe-C grains grow in the form of graphite nodules surrounded by an austenite shell, the growth is controlled primarily by the solid state diffusion of carbon through the iron shell and therefore depends on the radius R of the grain itself and possibly on the radius R_c of the graphite nodule.

Su *et al.*[43] have defined the relationship between the growth rate and undercooling assuming a stationary concentration profile within the austenite layer as

$$V_s = \frac{1}{K_c} \cdot \frac{\Delta T_{E,c}}{R(R/R_c - 1)} \tag{27}$$

In many eutectic alloys, such as the Fe-C and the Al-Si types, which are of great interest for technical applications, the branching of lamellae or fibres is made difficulty by the presence of one or two faceted phases[44]. This results in irregular eutectic morphologies, where the phases are no longer parallel and regularly spaced. Based on experimental observations of directionally solidified Fe-C alloys, Jones *et al.*[45] found that the average value, $\bar{\lambda}$, is given by

$$\bar{\lambda}^2 \cdot V_s = \phi^2 \cdot K_r / K_c \tag{28}$$

where ϕ is a constant (ϕ is close to 4 and 2 for Fe-C and Fe-Fe_3C alloys, respectively).

Dendritic and cellular are general crystal morphologies for the noneutectic alloys in the nonequilibrium conditions. Trivedi *et al.*[28,37,46] have established a model which includes growth rate and dynamic effect at the interface. This theory considers comprehensively the action of solute distribution, latent heat release and interface curvature, and gives a quantitative relationship between growth rate, undercooling and dendrite tip curvature at high growth rate[46],

$$\begin{aligned} \Delta T = (\frac{\Delta H}{C_L}) \cdot Iv(P_t) + \frac{k_v \cdot \Delta T_o^v \cdot Iv(P_c)}{1-(1-k_v)\cdot Iv(P_c)} + \\ (m - m_v) \cdot C_o + \frac{2\Gamma}{R} + \frac{V}{\mu_k} \\ \Delta T_o^v = m_v \cdot C_o \cdot (k_v - 1)/k_v \\ V \cdot R^2 \cdot (\frac{k_v \cdot \Delta T_o^v}{\Gamma \cdot D_i}) \cdot [\frac{1}{1-(1-k_v)\cdot Iv(P_c)}] \cdot \xi_c + \\ V \cdot R^2 \cdot (\frac{\Delta H}{C_L \cdot a_L \cdot \beta}) \cdot \xi_L = \frac{1}{\sigma^*} \end{aligned} \tag{29}$$

where P_t is thermal Peclet number, μ_k is interface kinetics coefficient.

A knowledge of the growth law of the dendrite tip, *i.e.* the relationship among $\Delta T_{L,c}$, V_s and R_t is not in itself sufficient to predict the final microstructural features and the cooling curves, since one still needs to predict how the solid fraction 'behind' the tip changes with temperature. Trivedi[47] has obtained the equation of the primary trunk spacing λ_1 by assuming that the primary trunk spacing is primarily influenced by thermal diffusion as

$$\lambda_1^2 = 224(2D_i \cdot \Gamma)^{1/2} \cdot G^{-1} \cdot V_t^{-1} \cdot R_t^{-1} \tag{30}$$

where R_t and V_t are the dendrite tip radius and growth rate of dendrite tip respectively.

Although the original secondary arm spacing , which develops close to the final value λ_2, which is ultimately observed on a metallographic section, is mainly a result of competitive growth and coarsening of the branches[44]. A model for secondary arm spacing which is frequently applied to Al based alloys is that developed by Feurer *et al.*[48]. It accounts for concentration variations in the liquid during solidification and gives the following relationship

$$\lambda_2^3 = M' \cdot \frac{\ln(C_e/C_o)}{(C_e - C_o) \cdot t_f} \tag{31}$$

where M' is a coarsening rate constant, t_f is the local solidification time.

Liu *et al.*[49] have studied the arm spacing at large range of solidification rate in directional solidification. Their results proved that the secondary arm spacing agrees with the equation $\lambda = A \cdot (G_L \cdot R)^{-B}$, A and B are constant.

Besides above mentioned nonequilibrium theories, there are also many others corresponding to various specific solidification technologies, for example, the nucleation and growth of laser melting alloys[50,51], the formation of the microstructure in rapid solidification powders[52,53] and the solidification of spray deposited preform and melt strip[54,55].

6. Future Developments

The phenomena of nonequilibrium solidification have been recently described on the dynamic and thermodynamics, and many theoretical models have been suggested, which make it possible to control and predict the process of solidification. Although most of the basic concepts are already outlined, they are not yet systematically implemented into solidification modeling codes. This is probably due to the fact that it is difficult to make a comprehensive view of the complex microscopic mechanisms which control solidification process. Therefore, this field of research is still in an early stage of development.

The researches of solidification theory in the future will be focused on the following sections: (1) A more accurate assessment for the theoretical model will be suggested; (2) A systematic comparison with experiment should be made; (3) Microstructural features as an important part of the predicting results must be included in the theoretical model; (4) The thermophysical properties of the alloys in nonequilibrium

solidification should be measured, and the relationship between thermophysical properties and temperature should be established as well; (5) The effects of diffusion coefficient and interface dynamic depended temperature on the interface stability should be considered; (6) The models for the interdendritic eutectic solidification of dendrite alloys and for the primary phase solidification of eutectic alloys should be established; (7) More complex systems should be considered such as ternary or technical alloys.

REFERENCES

[1] D.Turnbull and J.C.Fisher: *J. Chem. Phys.*, 1949, **17,** 71.

[2] J.D.Hunt: *Mater. Sci. Eng.*, 1984, **65,** 75.

[3] I.Dustin and W.Kurz: *Z. Metallkd.*, 1986, **77,** 265.

[4] M.Rappaz and D.M.Stefanescu: *Solidification Processing of Eutectic Alloys*, ed. D.M.Stefanescu, Warrendale, PA, Metallurgical Society of AIME, 1988, 133.

[5] W.Oldfield: *Trans. ASM*, 1966, **59,** 945.

[6] Ph.Thevoz, J.L.Desbiolles and M.Rappaz: *Metall. Trans.*, 1989, **20A,** 311

[7] Ph.Thevoz, J.L.Desbiolles and M.Rappaz: *Solidification Processing*, London, The Institute of Metals, 1988, 168.

[8] K.F.Kelton and A.L.Greer: *J. Non-Cryst. Solids*, 1986, **79,** 295.

[9] G.S.Shao and P.Tsakiropoulos: *Acta Metall. Mater.*, 1994, **42,** 2937.

[10] N.J.E.Adkins N.Saunders and P.Tsakiropoulos: *Mater. Sci. Eng.*, 1988, **98,** 217.

[11] Guosheng SHAO and Ningfu SHEN: *Progress of Materials Science*, 1992, **6,** 393. (in Chinese)

[12] Y.L.Tang and N.F.Shen: *J. Alloys Compounds*, 1993, **201,** L21.

[13] Shaokang GUAN, Yali TANG, Ningfu SHEN and Hanqi HU: *Acta Metall. Sin.*, 1994, **30,** A150. (in Chinese)

[14] R.Trivedi and W.Kurz: *Int. Mater. Rev.*, 1994, **39**(2), 49.

[15] J.C.Baker and J.W.Cahn: *Solidification*, Metals Park, OH, American Society for Metals, 1971, 23.

[16] W.J.Boettinger, S.R.Coriell and R.Trivedi: Proc. 4th Conf. on *Rapid Solidification'*, Baton, LA, Claitors Publishing Division, 1988, 13.

[17] J.C.Baker and J.W.Cahn: *Acta Metall.*, 1969, **17,** 575.

[18] M.J.Aziz: *J. Appl. Phys.*, 1982, **53,** 1158.

[19] M.J.Aziz: *Mater. Sci. Eng.*, 1988, **98,** 369.

[20] K.Y.Chen, Q.C.Li and J.Q.Guo: *J. Appl. Phys.*, 1991, **69**(10), 7325.

[21] H.Haken: *Synergetics*, Springer, Berlin, 1977, 89.

[22] J.Q.Guo, G.D.Gu and Q.C.Li: *Mater. Sci. Eng.*, 1988, **102A,** L5.

[23] Shenqiang WANG, Qingchun LI and Junqing GUO: Proc. Chin. Symp. on *Microgravity Science and Application*, Suzhou, 1991, 5. (in Chinese)

[24] W.W.Mullins and R.F.Sekerka: *J. Appl. Phys.*, 1964, **35,** 444.

[25] P.G.Zielinski and D.G.Ast: *J. Mater. Sci. Lett.*, 1983, **2,** 495.

[26] J.S.Langer and H.Muller-Krumbhaar: *Acta Metall.*, 1978, **26,** 1681.

[27] J.Lipton, M.E.Glickman and W.Kurz: *Mater. Sci. Eng.*, 1984, **65,** 57.

[28] R.Trivedi and W.Kurz: *Acta Metall.*, 1986, **34,** 1663.

[29] Shenqiang WANG, Qingchun LI and Jun JIA: Chin. Symp. Proc. on *Microgravity Science and Application*, Suzhou, 1991, 95.

[30] W.Kurz, B.Giovanola and R.Trivedi: *Acta Metall.*, 1986, **34,** 823.

[31] S.Z.Lu and J.D.Hunt: *J. Cryst. Growth*, 1992, **123,** 2135.

[32] R.Trivedi and W.Kurz: *Acta Metall. Mater.*, 1994, **42,** 15.

[33] Jianguo LI, Xiemin MAO and Hengzhi FU: *Acta Metall. Sin.*, 1990, **26**(4), A309. (in Chinese)

[34] Weidong HUANG and Yaohe ZHOU: *Acta Metall. Sin.*, 1991, **27**(2), A86. (in Chinese)

[35] S.Gill and W.Kurz: *Acta Metall. Mater.*, 1993, **41,** 3563.

[36] M.Gremaud, M.Carrard and W.Kurz: *Acta Metall. Mater.*, 1991, **39,** 1431.

[37] W.Kurz and R.Trivedi: *Acta Metall.*, 1990, **38,** 1.

[38] M.Carrard, M.Gremaud, M.Zimmermann and W.Kurz: *Acta Metall. Mater.*, 1992, **40,** 983.

[39] G.J.Merchant, R.J.Braun, K.Brattkus and S.H.Davis: *SIAM J. Appl. Math.*, 1992, **52,** 1279.

[40] A.Karma and A.Sarkissian: *Phys. Rev. Lett.*, 1992, **68,** 2616.

[41] R.Trivedi, P.Magnin and W.Kruz: *Acta Metall.*, 1987, **35,** 971.

[42] D.G.McCartney, J.D Hunt and R.M.Jordan: *Metall. Trans.*, 1980, **11A,** 1243.

[43] K.C.Su, I.Ohnaka, I.Yamauchi and T.Fuksako: *The Physical Metallurgy of Cast Iron*, ed. H.Fredriksson and M. Hillert, Mater. Res. Soc. Symp. Proc., New York, North-Holland, 1985, 34, 181.

[44] W.Kurz and D.J.Fisher: *Fundamentals of Solidification*, Aedermannsdorf, Switzerland, Trans. Tech. Pub., 1986.

[45] H.Jones and W.Kurz: *Z. Metallkd.*, 1981, **72,** 792.

[46] R.Trivedi, J.Lipton and W.Kurz: *Acta Metall.*, 1987, **35,** 965.

[47] R.Trivedi: *Metall. Trans.*, 1984, **15A,** 977.

[48] U.Feurer and R.Wunderlin: Einfluss der Zusammensetzung und der Erstarrungsbedingungen für die Dendritenmorphologie binärer Al-Legieierungen, Fachbericht der Deutschen Gessellschaft für Metallkunde, Oberursel, 1977.

[49] Siyuan LIU, Jianguo LI and Hengzhi FU: *Acta Metall. Sin.*, 1995, **31**(7), A329. (in Chinese)

[50] S.C.Gill, M.Zimmermann and W.Kurz: *Acta Metall. Mater.*, 1992, **40**(11), 2895.

[51] M.Gremaud, D.R.Allen, M.Rappaz and J.H.Perepezko: *Acta Mater.*, 1996, **44(7),** 2669.

[52] C.G.Levi and R.Mehrabian: *Metall. Trans.*, 1982, **13A,** 221.

[53] S.G.Kim, S.H.Shin, T.Suzuki and T.Umeda: *Metall. Mater. Trans.*, 1994, **25A,** 2815.

[54] Chengsong CUI, Zhuling JIANG, Jun SHEN and Qingchun LI: *Acta Metall. Sin.*, 1994, **30B**(7), 294. (in Chinese)

[55] R.F.Cochrane, P.V.Evans and A.L.Greer: *Mater. Sci. Eng.*, 1988, **98,** 99.